Experimental and theoretical study of the triple-differential cross section for electron-impact ionization of thymine molecules

S. M. Bellm,[1,*] C. J. Colyer,[1] B. Lohmann,[1] and C. Champion[2]

[1]*ARC Centre of Excellence for Antimatter-Matter Studies, The University of Adelaide, Adelaide, SA 5005, Australia*

[2]*Laboratoire de Physique Moléculaire et des Collisions, ICPMB (FR CNRS 2843), Institut de Physique, Université Paul Verlaine-Metz, 1 rue Arago, FR-57078 Metz Cedex 3, France*

(Received 12 December 2011; published 17 February 2012)

Triply differential cross sections for the electron-impact ionization of inner valence orbitals of thymine have been measured using the (*e*,2*e*) technique at an incident electron energy of 250 eV. The measurements have been performed with coplanar asymmetric kinematics for scattered electron angles of –10° and –15° and with an ejected-electron energy of 20 eV. Theoretical calculations have been performed within the first-order Born approximation and are in very good agreement with the experimental data.

DOI: 10.1103/PhysRevA.85.022710 PACS number(s): 34.80.Gs

I. INTRODUCTION

In recent years, extensive research has been undertaken into the study of radiation damage in biomolecular systems [1,2]. The discovery that large numbers of low-energy secondary electrons, which are formed along the track of high-energy ionizing particles, play a major role in the damage to DNA [3] has further motivated the investigation of electron interactions with molecules of biological importance. The majority of these low-energy secondary electrons have initial kinetic energies of 20 eV [4] or less. It has been determined that low-energy electrons can cause significant damage to DNA through the process of dissociative attachment, which occurs even at energies well below ionization thresholds. This occurs as a result of the formation of ionic products or free radicals, which may then chemically react with DNA leading to strand breaking. Indeed it is now recognized that much of the cellular damage initiated by high-energy radiation results through this mechanism [5].

There has also been great interest in studying radiation damage in biological systems using Monte Carlo based track structure codes to describe the nature of damage resulting from high-energy incident radiation [6–10]. Cross-section data are essential to these simulations. To further our understanding of the reactions leading to DNA and RNA damage, spectroscopic and cross-section values for electron impact on DNA and RNA are needed. The electron-electron coincidence ionization technique or (*e*,2*e*) technique can be used to provide spatial information about the scattering direction of electrons. In the (*e*,2*e*) technique, a projectile electron with well defined energy and momentum ionizes an atomic or molecular target. The scattered projectile and ejected target electron are detected in time coincidence with their energies and momenta determined, yielding a multiply differential cross section termed the triple-differential cross section (TDCS). The method can be used to determine information about the ionization dynamics of atomic and molecular targets as well as to elucidate details about the bound electronic structure of the target, which is known as electron momentum spectroscopy (EMS).

Thymine ($C_6H_6N_2O_2$) is one of the four nucleobases found in DNA, along with adenine, guanine, and cytosine. Thymine and cytosine are both pyrimidine derivatives while adenine and guanine are purine derivatives. Due to its similarity to the nucleobase ring systems, pyrimidine has been used as a model compound to investigate electron collisions with DNA constituents. To our knowledge no previous (*e*,2*e*) measurements have been reported in the literature for thymine, however, pyrimidine has been studied by EMS to investigate the molecular structure [11,12]. Recently Dal Cappello *et al*. have published preliminary calculations of the triple-differential cross section for electron-impact ionization of thymine, performed within the first Born approximation and in the second-order Born approximation [13]. A number of studies have investigated elastic scattering from thymine. These include theoretical studies concerning electron scattering from the DNA bases by Mozejko and Sanche [14], and Blanco and Garcia [15]. In these studies elastic cross sections for all of the DNA and RNA bases were calculated, differential in both energy and in angle. Relative elastic differential cross sections (DCS) for thymine and cytosine have also recently been measured experimentally using the crossed beam method [16]. Triple-differential cross sections, however, provide the most complete information about the details of the ionization of atomic and molecular targets, which is essential to modeling the deposition of energy in biological matter.

Experimental difficulties associated with TDCS measurements for molecular targets occur due to the difficulties of experimentally resolving different molecular electronic states. A number of molecules for which experimental dynamical (*e*,2*e*) studies have been undertaken are listed in Ref. [17]. Molecular orbitals are often, depending on the molecular configuration of the target, quite closely spaced in energy and contributions from vibrational and rotational states can further complicate the measurements. In addition, theory has had to deal with modeling polyatomic target species, with many of the approximations that work for the atomic case breaking down due to the polycentric nature of some of these molecules. Madison and Al-Hagan [18] have reviewed some of the recent theoretical work that has been performed. Here we present triple-differential cross sections for electron-impact ionization of a combination of inner valence orbitals of thymine.

*susan.bellm@flinders.edu.au

II. EXPERIMENTAL APPARATUS

Coplanar asymmetric measurements were performed using a conventional coincidence spectrometer. The experimental apparatus has previously been described in detail [19,20]. Briefly, electrons produced by thermionic emission from a tungsten filament are collimated and transported to the interaction region using five cylindrical electrostatic lens elements. The resulting electron beam energy resolution is approximately 0.5 eV. The electron beam then crosses a molecular target beam.

Thymine is a powder at room temperature and gaseous thymine is produced using a molecular beam oven, centrally located in the spectrometer. The oven is capable of being heated to temperatures in excess of 220 °C through the use of two independent Thermocoax heating elements. The effusion temperatures which were used in the present measurements were 140 °C–150 °C, well below the decomposition temperature of thymine of about 335 °C. A liquid-nitrogen-filled cold finger, located concentric above the interaction volume, was used to trap thymine, to help prevent it from condensing on the vacuum chamber and electron optics. The cold finger is constructed from 310 stainless steel with an oxygen-free high thermal conductivity copper collection disk at the end and is filled externally with liquid nitrogen. To further prevent the deposition of thymine affecting the measurements, the electrostatic lens elements closest to the interaction region were cleaned at regular intervals during the measurements.

The molecular target beam is oriented perpendicular to the scattering plane, which is defined by the momentum vectors of the incident and measured outgoing electrons. The higher-energy (scattered) and lower-energy (ejected) outgoing electrons are both detected in hemispherical electron energy analyzers, each comprising a five-element electrostatic entrance lens system, hemispherical selector, and channel electron multiplier detector. Coincidence timing procedures [21] are used to identify, from the relative arrival times of electrons at the two detectors, if the two detected electrons are correlated and originate from the same scattering event. Background events are subtracted using standard statistical methods. The two electron energy analyzers are mounted on independent turntables concentric with the interaction region. The detection energies of the hemispherical electron energy analyzers have been calibrated using the $L_{2,3}M_{2,3}M_{2,3}$ Auger spectrum of argon [22], while the angular calibration of the analyzers has been determined using the well-defined minimum in the differential cross section for elastic scattering of 60 eV electrons from argon [23].

In dynamical TDCS measurements, the scattered electron is detected at a fixed forward angle (θ_a) with respect to the incident electron beam direction, while ejected-electron angular distributions are measured by scanning the ejected-electron energy analyzer and detecting electrons at a number of different ejected-electron angles (θ_b) within the scattering plane. The experiments were performed at an incident electron energy of 250 eV and an ejected-electron energy of 20 eV. The energy of the scattered electron is determined by conservation of energy such that

$$E_0 = E_a + E_b + \varepsilon_b, \tag{1}$$

where E_0, E_a, and E_b are the kinetic energies of the incident, scattered, and ejected electrons, respectively, and ε_b is the binding energy of the orbital that is ionized. To verify that the instrument was functioning correctly, the TDCS for the ionization of the helium 1s orbital was measured and compared to distorted wave Born approximation calculations (DWBA) under the same kinematics, which are known to produce accurate results.

III. THEORETICAL FRAMEWORK

The cross sections presented in this work have been calculated in the first Born approximation (FBA) framework by using a theoretical model developed in the partial-wave formalism (see, for example, Champion *et al.* [24,25]). In these studies, several models were tested for improving the description of the final state: (i) the Coulomb Born approximation (CBA) model (in which the ejected electron is described by a Coulomb wave, whereas the incident and the scattered electrons are described by plane waves); (ii) the distorted wave Born approximation (DWBA) model in which the ejected electron was described by means of a distorted wave function calculated by numerical resolution of the Schrödinger equation where distortion effects between the ejected species and the ionized target were introduced; (iii) the two-Coulomb-wave (2CW) model where the scattered and the ejected electrons were both described by target Coulomb waves; and finally (iv) the BBK model (see Brauner *et al.* [26]) where the final state is described by the product of three Coulomb waves, which take into account the interaction between the scattered electron and the residual target, that between the ejected electron and the residual target and that between the scattered electron and the ejected one, respectively. However, as explained in Champion *et al.* [24], all these sophisticated descriptions are essentially needed for experimental configurations in which the ejected velocity v_e matches the scattered velocity v_s and consequently do not concern the case here investigated.

In the present work the collision is described in the independent electron model by employing the Coulomb Born approximation, which is completely justified under the present kinematics (see, for example, Whelan *et al.* [27] or McCarthy and Weigold [28]). Indeed, the initial state is constituted by an energetic particle ($E_0 = 250$ eV), i.e., with a kinetic energy at least ten times greater than the ionization energies of the molecular orbitals investigated. Concerning the final state, the scattered electron has a kinetic energy E_a of the same order as the energy of the incident energy E_0, i.e., at least ten times greater than the ejected particle E_b. Under these conditions the initial state can be described as a product of a plane wave function for the incident electron with a molecular target wave function. In the final state, the ejected electron is represented by a Coulomb wave function, whereas the scattered electron is described by a plane wave function. Moreover, due to the large asymmetry of the collision energies (an ejected-electron energy of $E_b = 20$ eV and a scattered-electron energy E_a greater than 210 eV), we do not introduce the exchange effect in the TDCS calculations.

Moreover, it will be assumed that the *passive* (not ionized) electrons will remain as frozen in their molecular orbitals

TABLE I. Population and binding energies of the thymine molecular orbitals.

Molecular orbital	Ionization energies (eV)	Population
1	9.14	1.12 C($2p$) + 0.46 N($2p$) + 0.34 O($2p$) + 0.08 H($1s$)
2	10.93	0.90 N($2p$) + 1.08 O($2p$) + 0.02 C($2p$)
3	11.35	1.46 O($2p$) + 0.20 N($2p$) + 0.26 C($2p$) + 0.02 C($2s$)
4	12.13	1.44 O($2p$) + 0.20 N($2p$) + 0.22 C($2p$) + 0.04 N($2s$) + 0.04 H($1s$)
5	13.29	0.60 N($2p$) + 0.50 O($2p$) + 0.12 H($1s$) + 0.76 C($2p$)
6	14.47	1.06 C($2p$) + 0.70 H($1s$) + 0.14 O($2p$)
7	14.68	0.52 O($2p$) + 0.76 C($2p$) + 0.58 N($2p$) + 0.12 H($1s$)
8	14.81	1.32 C($2p$) + 0.22 O($2p$) + 0.12 N($2p$) + 0.08 C($2s$) + 0.14 H($1s$)
9	15.57	1.18 C($2p$) + 0.48 H($1s$) + 0.24 O($2p$) + 0.08 N($2p$)
10	15.99	0.84 O($2p$) + 0.14 O($2s$) + 0.68 C($2p$) + 0.18 H($1s$) + 0.08 N($2p$)
11	16.36	0.96 O($2p$) + 0.26 O($2s$) + 0.56 C($2p$) + 0.02 C($2s$) + 0.06 H($1s$) + 0.06 N($2p$)
12	17.44	0.58 O($2p$) + 0.48 C($2p$) + 0.34 N($2p$) + 0.20 O($2s$) + 0.24 H($1s$) + 0.10 C($2s$)
13	17.62	0.90 C($2p$) + 0.82 N($2p$) + 0.26 O($2p$)
14	18.59	0.76 N($2p$) + 0.52 C($2p$) + 0.54 H($1s$) + 0.06 C($2s$) + 0.02 O($2p$)
15	20.28	0.88 N($2p$) + 0.40 C($2p$) + 0.34 H($1s$) + 0.26 C($2s$) + 0.08 O($2p$) + 0.04 O($2s$)
16	20.38	0.62 N($2p$) + 1.06 C($2p$) + 0.16 O($2p$) + 0.04 C($2s$)
17	23.51	0.90 N($2p$) + 0.38 C($2s$) + 0.30 C($2p$) + 0.12 H($1s$) + 0.12 O($2s$) + 0.06 N($2s$) + 0.06 O($2p$)
18	24.08	0.50 N($2p$) + 0.64 C($2s$) + 0.46 C($2p$) + 0.22 H($1s$) + 0.06 N($2s$) + 0.04 O($2s$) + 0.02 O($2p$)
19	25.53	1.24 C($2s$) + 0.24 N($2p$) + 0.20 C($2p$) + 0.22 H($1s$) + 0.04 O($2s$)
20	29.23	1.44 C($2s$) + 0.12 N($2s$) + 0.22 C($2p$) + 0.04 N($2p$) + 0.06 O($2s$)
21	32.65	1.52 N($2s$) + 0.12 O($2s$) + 0.12 C($2s$) + 0.12 C($2p$) + 0.10 H($1s$)
22	34.46	1.04 N($2s$) + 0.52 O($2s$) + 0.20 C($2s$) + 0.12 C($2p$) + 0.08 N($2p$) + 0.04 H($1s$)
23	37.09	1.40 O($2s$) + 0.34 C($2s$) + 0.18 O($2p$) + 0.04 N($2p$) + 0.02 N($2s$)
24	37.85	0.92 O($2s$) + 0.38 C($2s$) + 0.46 N($2s$) + 0.14 O($2p$) + 0.02 N($2p$) + 0.02 C($2p$)
25	293.56	1.98 C($1s$)
26	294.27	1.98 C($1s$)
27	296.03	1.98 C($1s$)
28	297.42	2.00 C($1s$)
29	298.44	2.00 C($1s$)
30	408.28	1.98 N($1s$)
31	408.68	1.98 N($1s$)
32	536.74	2.00 O($1s$)
33	536.87	1.98 O($1s$)

during the collision. Thus, in the laboratory framework, the triply differential cross sections, namely, differential in the direction of the scattered projectile Ω_s, differential in the direction of the ejected electron Ω_e, and differential in the ejected energy E_e and denoted in the following $\sigma^{(3)}(\Omega_s,\Omega_e,E_e)$ can be written as

$$\sigma^{(3)}(\Omega_s,\Omega_e,E_e) \equiv \frac{d^3\sigma}{d\Omega_s d\Omega_e dE_e} = \sum_{j=1}^{N} \frac{d^3\sigma_j}{d\Omega_s d\Omega_e dE_e}$$
$$\equiv \sum_{j=1}^{N} \sigma_j^{(3)}(\Omega_s,\Omega_e,E_e), \qquad (2)$$

where N is the number of molecular orbitals used in the complete neglected differential overlap (CNDO) description of the DNA thymine base ($N = 33$).

In this context, the input parameters for the occupied molecular orbitals of thymine were obtained by using an *ab initio* method. Total-energy calculations were performed in the gas phase with the Gaussian 09 software at the RHF/3-21G level of theory [29]. The computed ionization energies of the occupied molecular orbitals of the nucleobase were scaled so that their calculated Koopmans ionization energy, i.e., the ionization energy of their highest occupied molecular orbital (HOMO) coincides with the experimental value of the ionization potential measured by Hush and Cheung [30]. For each molecular orbital (MO) labeled j, the effective number of electrons $\xi_{j,i}$ relative to the atomic component i was derived from a standard Mulliken population analysis and their sum for each occupied MO is very close to 2, since only atomic shells with very small population have been discarded (see Table I).

Thus, the triply differential cross section of each molecular orbital labeled j can be expressed as a weighted sum of atomic triply differential cross sections $\sigma_{at,i}^{(3)}$ corresponding to the different atomic components involved in the molecular subshell. Thus, we write

$$\sigma_j^{(3)}(\Omega_s,\Omega_e,E_e) = \sum_i \xi_{j,i}\sigma_{at,i}^{(3)}(\Omega_s,\Omega_e,E_e). \qquad (3)$$

Thus, the triply differential cross sections $\sigma_{at,i}^{(3)}$ are calculated by using the well-known expression

$$\sigma_{at,i}^{(3)}(\Omega_s,\Omega_e,E_e) = (2\pi)^4 \frac{k_s k_e}{k_i} |[T_{a,b}]_i|^2, \qquad (4)$$

where $[T_{a,b}]_i$ denotes the atomic transition matrix element between an initial state a and a final state b and is given by

$$[T_{a,b}]_i = \langle \phi_{i,b}(\mathbf{R})\varphi_{i,b}(\mathbf{r})|\frac{1}{R} - \frac{1}{|\mathbf{R}-\mathbf{r}|}|\phi_{i,a}(\mathbf{R})\varphi_{i,a}(\mathbf{r})\rangle, \quad (5)$$

where $\mathbf{R}$ and $\mathbf{r}$ give the positions of the projectile and of the active electron, respectively, $\phi_{i,a}(\mathbf{R})$ and $\phi_{i,b}(\mathbf{R})$ refer to the plane waves used for describing the incoming and the outgoing projectile, respectively, and $\varphi_{i,b}(\mathbf{r})$ stands for the ejected-electron Coulomb wave function. $\varphi_{i,a}(\mathbf{r})$ represents the atomic wave function of the ith orbital used in the CNDO expansion of each target molecular subshell. These atomic wave functions essentially refer to C_{2p}, N_{2s}, N_{2p}, and O_{2p} ones and are expanded on a spherical harmonic basis with a radial part given in terms of Slater functions, namely,

$$\varphi_{i,a}(\mathbf{r}) = \sum_{k=1}^{N_i} \frac{(2\varsigma_k)^{n_{ik}+1/2}}{\sqrt{(2n_{ik})!}} r^{n_{ik}-1} e^{-\varsigma_{ik}r} Y_{l_{ik}m_{ik}}(\Omega_r)$$
$$\equiv \sum_{k=1}^{N_i} f_{ik}(r) Y_{l_{ik}m_{ik}}(\Omega_r), \quad (6)$$

where N_i denotes the number of partial waves (n_{ik},l_{ik},m_{ik}) used for the description of the ith atomic orbital. For more details about these coefficients, we refer the reader to the Clementi's tables of atomic functions [31].

In Eq. (3), $\boldsymbol{k_i}$, $\boldsymbol{k_s}$, and $\boldsymbol{k_e}$ represent the wave vectors of the incident electron, the scattered electron, and the ejected electron, respectively.

IV. RESULTS AND DISCUSSION

Figure 1 shows the binding energy spectrum for the valence region of thymine. The incident and ejected-electron energies were fixed at 250 eV and 20 eV, respectively, while the scattered electron energy was scanned across a range of energies. The detection angles for the scattered and ejected electrons were chosen to be $-10°$ and $75°$, respectively. The instrumental binding energy resolution under the chosen conditions was estimated to be 1.5 eV FWHM, from the width of the helium 1s binding energy peak measured under the same kinematics. The binding energy spectrum has been fitted with a sum of nine Gaussian functions of fixed width. As the binding energy resolution is comparable to the natural width of a number of orbitals observed in photoelectron spectra of thymine [32], the width of the individual peaks in the Gaussian fitting was determined by adding the coincidence resolution and the natural widths of each orbital in quadrature.

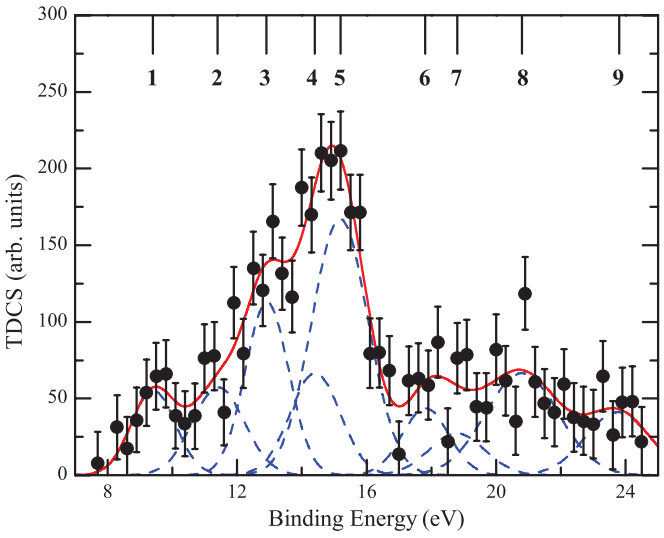

FIG. 1. (Color online) Measured binding energy spectrum for the valence region of thymine. The data have been fitted with a sum of Gaussian functions, using a convolution of the coincidence binding energy resolution and the natural width of the molecular orbitals to define the peak width parameters.

Thymine exists in two conformers which differ in the orientation of the methyl group that is attached to the hexagonal ring. Only the *cis* conformer is a rotational minimum; the *trans* conformer is a transition state [33]. There is no difference in orbital assignments and momentum profiles for the two conformers as the differences in orbital ionization energies between the structures are very small, and there is no change in molecular symmetry between them.

The HOMO of thymine is the $6a''$ state at a binding energy of 9.4 eV and is separated by 1.8 eV from the HOMO-1 orbital. The HOMO of thymine is delocalized, but dominated by contributions from bonding carbon to carbon and the nitrogen to carbon antibonding π orbitals [34]. The largest peak in the binding energy spectrum occurs at 14.5 eV and has been fitted with two Gaussian functions. It is thought to contain contributions from eight molecular orbitals. Based on the photoelectron spectroscopy measurements (PES) of Trofimov *et al.* [32], it is likely that the $2a''$ and $14a'$ orbitals are the major contributors, but contributions from other orbitals are also likely to occur.

Experimental and theoretical TDCSs for electron-impact ionization of the combined $14a'$ and $2a''$ orbitals at a binding energy of 14.5 eV and a scattered electron angle of $-15°$ are presented in Fig. 2. The angular distributions can be divided into both the binary region, which ranges from $0°$ to $180°$, and the recoil region, which extends between $180°$ and $360°$. Structure in the binary region occurs due to single binary collisions and depending upon the kinematics it may contain strong signatures of the orbital structure [35]. The recoil region contains structure arising from processes in which the ejected electron first undergoes a binary collision, followed by elastic backscattering from the residual ion. The distribution has a binary lobe centered along the momentum transfer direction (+**K**) and a recoil lobe pointing in the opposite direction (–**K**). Following from the types of orbital assigned in Table II, it is expected that at smaller recoil ion momenta, the contribution to the momentum density probability distribution from the $14a'$ orbital (s-type) will be greater than that of the $2a''$ (p-type). At larger recoil ion momenta the relative contribution from the $2a''$ orbital will increase. Under the present kinematics this corresponds to ejected-electron angles around the momentum transfer direction where the $14a'$ state can be expected to dominate, while increased contributions from the $2a''$ state are expected at larger ejected-electron angles of around $120°$.

The present theoretical calculations match the experimental data quite well in both the binary and recoil regions. As the experimental data are relative they have been normalized to

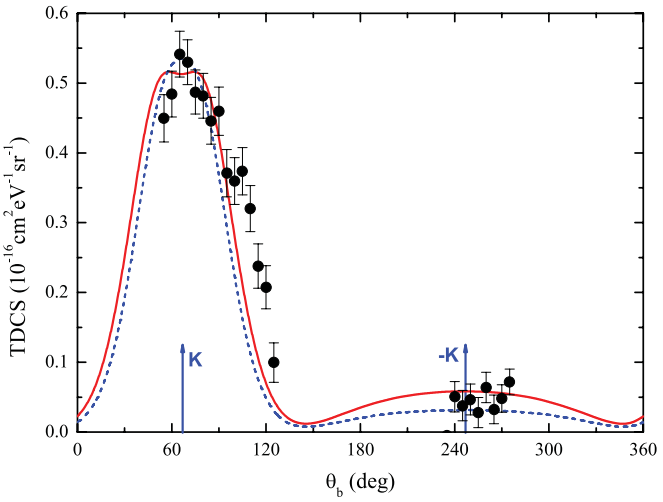

FIG. 2. (Color online) The triple-differential cross sections for ionization of the combined $2a''+14a'$ inner valence orbital of thymine with $E_0 = 250$ eV and $E_b = 20$ eV. The scattered electron detection angle is -15° and $|\mathrm{K}| = 1.12$ a.u. The positions of the momentum transfer vector, $+\mathbf{K}$, and $-\mathbf{K}$ are indicated by the arrows. Points are the experimental data. Solid curve (red): Calculation for the $2a''$ orbital. Dashed curve (blue): Calculation for the $14a'$ orbital. The calculation for the $14a'$ orbital has been scaled by a factor of 0.6 (see text for details).

the calculation for the $2a''$ orbital to give the best visual fit to the data. The calculation for the $14a'$ orbital has been scaled by a factor of 0.6 to facilitate comparison with the experimental data. In particular, the calculation for the $2a''$ orbital predicts the shape and relative intensities of the binary and recoil peaks quite well. A small recoil peak is expected as at the -15° scattered electron angle the reaction kinematics is very close to that of Bethe ridge conditions. Under these conditions all momentum is transferred to the bound, stationary target electron during the collision, the ion plays no role, and almost no recoil lobe is expected. The $2a''$ calculation does, however, show a small splitting of the binary peak, whereas a single binary peak is observed in the experimental data. It is likely that this structure is not observed in the present experimental data because, as previously mentioned with the coincidence energy resolution of our apparatus, we are unable to resolve individual orbitals and, as detailed in Table II, contributions from a number of orbitals of both s-type and p-type character are likely to be present. The calculation for the $14a'$ orbital somewhat underestimates the width of the binary peak and the relative intensity of the recoil peak, but is still in good agreement with the experimental data.

Figure 3 shows the TDCS for electron-impact ionization of thymine at a scattered electron angle of -10°. The distribution appears very similar to that for the -15° scattered electron angle in Fig. 2, although the magnitude of the recoil peak relative to the magnitude of the binary peak is slightly greater than for the -15° case. The TDCS shows a single binary lobe centered close to the momentum transfer direction with a small shift of approximately 5° to larger ejected-electron angles. This is likely to be due to postcollisional ionization effects in which Coulomb repulsion between the two final state electrons causes a slight shift to the binary peak. Again absolute values are assigned to the experimental data by normalization of the data set to the FBA calculation for the $2a''$ orbital to achieve the best visual fit and the FBA calculation for the $14a'$ orbital has been scaled by a factor of 0.71.

Similar to the scattered electron angle of -15°, the FBA calculation for the $14a'$ orbital slightly underestimates the width of the binary peak and the relative magnitude of the recoil peak. The calculation for the $2a''$ orbital is again in impressive qualitative agreement with the measured data, especially given the complexity of the molecular target. We note, however, that absolute cross-section measurements are needed to assess how accurately the magnitudes of the

TABLE II. Binding energies for thymine in eV. The orbital assignments, calculations, and PES data are from Trofimov *et al.* (Ref. [32]).

Peak	Orbital	FWHM	Type	Present work	OVGF/6-311++G**	PES
1	$6a''$	1.6	π_6	9.4(0.6)	9.66	9.19
2	$5a''$	1.9	π_5	11.4(0.6)	11.88	10.45
	$18a'$		σ_{LPO}		12.24	10.14
	$17a'$		σ_{LPO}		13.12	10.89
3	$4a''$	1.6	π_4	12.9(0.6)	13.98	12.27
4	$16a'$	1.8	σ	14.4(0.6)	15.09	13.32
	$3a''$		π_3		15.29	
	$15a'$		σ		15.55	
	$2a''$		π_2		16.13	14.87
	$14a'$		σ		16.91	
5	$13a'$	2.1	σ	15.2(0.6)	17.57	15.58
	$12a'$		π_1		18.48	
	$1a''$		σ		18.14	
6	$11a'$	1.7	σ	17.8(0.6)	19.34	17.93
7	$10a'$	2.0		18.8(0.6)		
8	$9a'$	2.7		20.7(0.6)		20.85
9	$8a'$	2.3		23.8(0.6)		22.09
	$7a'$					
	$6a'$					

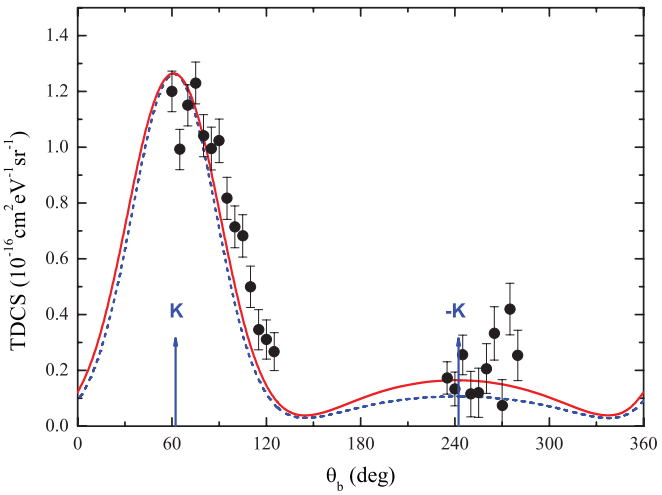

FIG. 3. (Color online) The triple-differential cross sections for ionization of the combined $2a'' + 14a'$ inner valence orbital of thymine with $E_0 = 250$ eV and $E_b = 20$ eV. The scattered electron detection angle is -10° and $|\mathbf{K}| = 0.78$ a.u. The positions of the momentum transfer vector, $+\mathbf{K}$, and $-\mathbf{K}$ are indicated by the arrows. Points are the experimental data. Solid curve (red): Calculation for the $2a''$ orbital. Dashed curve (blue): Calculation for the $14a'$ orbital. The calculation for the $14a'$ orbital has been scaled by a factor of 0.71 (see text for details).

predicted TDCSs reflect the true values. Traditionally, placing TDCS data on an absolute scale has been a complicated process [36,37]. A simple method for absolute $(e,2e)$ measurements was recently reported [37]. Unfortunately, however, due to the high density of molecular orbitals for a complex molecular target like thymine, these measurements would still be very difficult to perform.

V. CONCLUSIONS

In this paper we have presented experimental and theoretical $(e,2e)$ results for the triple-differential cross section for electron-impact ionization of the DNA nucleobase thymine. The measured binding energies and orbital assignment are in good agreement with previous PES data. The TDCSs at both scattered electron angles investigated exhibit a narrow binary peak. Both TDCSs also showed a small recoil peak relative to the magnitude of the binary peak, suggesting that there is very little interaction between the ejected electron and the target ion under these kinematical conditions. The calculations performed within the FBA framework were in very good agreement with the experimental data, successfully predicting the binary peak shape and the relative magnitudes of the binary and recoil peaks. The determination of spatial information about the scattering direction of electrons is an important step in the modeling of radiation damage in biological systems and as such the good agreement between experiment and theory supports the use of calculations performed within this framework in track structure modeling.

ACKNOWLEDGMENTS

This work was supported by the Australian Research Council Centre of Excellence for Antimatter-Matter Studies. C.J.C. would like to acknowledge scholarship support from the Australian Government.

[1] L. Sanche, Eur. Phys. J. D **35**, 367 (2005).
[2] L. Sanche, Mass Spectrom. Rev. **21**, 349 (2002).
[3] B. Boudaïffa, P. Cloutier, D. Hunting, M. A. Huels, and L. Sanche, Science **287**, 1658 (2000).
[4] V. Cobut, Y. Frongillo, J. P. Patau, T. Goulet, M. J. Fraser, and J. P. Jay-Gerin, Radiat. Phys. Chem. **51**, 229 (1998).
[5] B. Boudaïffa, P. Cloutier, D. Hunting, M. A. Huels, and L. Sanche, Radiat. Res. **157**, 227 (2002).
[6] C. Champion, Phys. Med. Biol. **48**, 2147 (2003).
[7] M. Fuss, A. Munoz, J. C. Oller, F. Blanco, P. Limao-Vieira, C. Huerga, M. Tellez, M. J. Hubin-Fraskin, K. Nixon, M. Brunger, and G. Garcia, in *XXVI International Conference on Photonic, Electronic and Atomic Collisions*, edited by A. E. Orel, A. F. Starace, D. Nikolic, N. Berrah, T. W. Gorczyca, E. Y. Kamber, and J. A. Tanis (IOP Publishing Ltd, Bristol, 2009), Vol. 194, p. 012028.
[8] D. T. Goodhead, Int. J. Radiat. Biol. **65**, 7 (1994).
[9] H. Nikjoo, S. Uehara, D. Emfietzoglou and F. A. Cucinotta, Radiat. Meas. **41**, 1052 (2006).
[10] A. Munoz, F. Blanco, G. Garcia, P. A. Thorn, M. J. Brunger, J. P. Sullivan, and S. J. Buckman, Int. J. Mass Spectrom. **277**, 175 (2008).
[11] C. G. Ning, K. Liu, Z. H. Luo, S. F. Zhang, and J. K. Deng, Chem. Phys. Lett. **476**, 157 (2009).
[12] S. H. R. Shojaei, B. Hajgato, and M. S. Deleuze, Chem. Phys. Lett. **498**, 45 (2010).
[13] C. Dal Cappello, Z. Rezkallah, S. Houamer, I. Charpentier, P. A. Hervieux, M. F. Ruiz-Lopez, R. Dey, and A. C. Roy, Phys. Rev. A **84**, 032711 (2011).
[14] P. Możejko and L. Sanche, Radiat. Environ. Biophys. **42**, 201 (2003).
[15] F. Blanco and G. Garcia, Phys. Lett. A **360**, 707 (2007).
[16] C. J. Colyer, S. M. Bellm, F. Blanco, G. García, and B. Lohmann, Phys. Rev. A **84**, 042707 (2011).
[17] C. J. Colyer, M. A. Stevenson, O. Al-Hagan, D. H. Madison, C. G. Ning, and B. Lohmann, J. Phys. B: At. Mol. Opt. Phys. **42**, 235207 (2009).
[18] D. H. Madison and O. Al-Hagan, J. At. Mol. Opt. Phys. **2010**, 367180 (2010).
[19] S. J. Cavanagh and B. Lohmann, J. Phys. B: At. Mol. Opt. Phys. **32**, L261 (1999).
[20] C. J. Colyer, S. M. Bellm, B. Lohmann, G. F. Hanne, O. Al-Hagan, D. H. Madison, and C. G. Ning, J. Chem. Phys. **133**, 124302 (2010).
[21] E. Weigold and I. E. McCarthy, *Electron Momentum Spectroscopy* (Kluwer Academic-Plenum, New York, 1999).
[22] L. O. Werme, T. Bergmark, and K. Siegbahn, Phys. Scr. **8**, 149 (1973).

[23] R. Panajotovic, D. Filipovic, B. Marinkovic, V. Pejcev, M. Kurepa, and L. Vuskovic, J. Phys. B **30**, 5877 (1997).
[24] C. Champion, C. Dal Cappello, S. Houamer, and A. Mansouri, Phys. Rev. A **73**, 012717 (2006).
[25] C. Champion, J. Hanssen, and P. A. Hervieux, J. Chem. Phys. **121**, 9423 (2004).
[26] M. Brauner, J. S. Briggs, H. Klar, J. T. Broad, T. Rosel, K. Jung, and H. Ehrhardt, J. Phys. B: At. Mol. Opt. Phys. **24**, 657 (1991).
[27] H. R. J. Walters, X. Zhang, and C. T. Whelan, in *(e,2e) and Related Processes*, edited by C. T. Whelan, H. R. J. Walters, A. Lahmam-Bennani, and H. Ehrhardt (Kluwer Academic, Boston, 1993), pp. 33–74.
[28] I. E. McCarthy and E. Weigold, Rep. Prog. Phys. **54**, 789 (1991).
[29] M. J. Frisch, G. W. Trucks, H. B. Schlegel, G. E. Scuseria, M. A. Robb, J. R. Cheeseman, G. Scalmani, V. Barone, B. Mennucci, G. A. Petersson, H. Nakatsuji, M. Caricato, X. Li, H. P. Hratchian, A. F. Izmaylov, J. Bloino, G. Zheng, J. L. Sonnenberg, M. Hada, M. Ehara, K. Toyota, R. Fukuda, J. Hasegawa, M. Ishida, T. Nakajima, Y. Honda, O. Kitao, H. Nakai, T. Vreven, J. A. Montgomery Jr., J. E. Peralta, F. Ogliaro, M. Bearpark, J. J. Heyd, E. Brothers, K. N. Kudin, V. N. Staroverov, R. Kobayashi, J. Normand, K. Raghavachari, A. Rendell, J. C. Burant, S. S. Iyengar, J. Tomasi, M. Cossi, N. Rega, J. M. Millam, M. Klene, J. E. Knox, J. B. Cross, V. Bakken, C. Adamo, J. Jaramillo, R. Gomperts, R. E. Stratmann, O. Yazyev, A. J. Austin, R. Cammi, C. Pomelli, J. W. Ochterski, R. L. Martin, K. Morokuma, V. G. Zakrzewski, G. A. Voth, P. Salvador, J. J. Dannenberg, S. Dapprich, A. D. Daniels, Ö. Farkas, J. B. Foresman, J. V. Ortiz, J. Cioslowski, and D. J. Fox, GAUSSIAN 09, Rev. A.02, Gaussian, Inc., Wallingford CT, 2009.
[30] N. S. Hush and A. S. Cheung, Chem. Phys. Lett. **34**, 11 (1975).
[31] E. Clementi, IBM J. Res. Develop. Suppl. **9**, 2 (1965).
[32] A. B. Trofimov, J. Schirmer, V. B. Kobychev, A. W. Potts, D. M. P. Holland, and L. Karlsson, J. Phys. B: At. Mol. Opt. Phys. **39**, 305 (2006).
[33] O. Dolgounitcheva, V. G. Zakrzewski, and J. V. Ortiz, J. Phys. Chem. A **106**, 8411 (2002).
[34] K. B. Bravaya, O. Kostko, M. Ahmed, and A. I. Krylov, Phys. Chem. Chem. Phys. **12**, 2292 (2010).
[35] H. Ehrhardt, K. Jung, G. Knoth, and P. Schlemmer, Z. Phys. D **1**, 3 (1986).
[36] A. Lahmam-Bennani, M. Cherid, and A. Duguet, J. Phys. B: At. Mol. Opt. Phys. **20**, 2531 (1987).
[37] L. R. Hargreaves, M. A. Stevenson, and B. Lohmann, Meas. Sci. Technol. **21**, 055112 (2010).